Journal of Electroanalytical Chemistry 875 (2020) 114070

Contents lists available at ScienceDirect

Journal of Electroanalytical Chemistry

journal homepage: www.elsevier.com/locate/jelechem

Characterizing intermolecular interactions in redox-active pyridinium-based molecular junctions

Songsong Li [a,d,e,1], Jialing Li [b,d,e,1], Hao Yu [b], Sanja Pudar [c], Bo Li [b], Joaquín Rodríguez-López [c,d,e], Jeffrey S. Moore [a,c,d,e], Charles M. Schroeder [a,b,c,d,e,*]

[a] Department of Materials Science and Engineering, University of Illinois at Urbana-Champaign, Urbana, IL 61801, United States
[b] Department of Chemical and Biomolecular Engineering, University of Illinois at Urbana-Champaign, Urbana, IL 61801, United States
[c] Department of Chemistry, University of Illinois at Urbana-Champaign, Urbana, IL 61801, United States
[d] Beckman Institute for Advanced Science and Technology, University of Illinois at Urbana-Champaign, Urbana, IL 61801, United States
[e] Joint Center for Energy Storage Research (JCESR), Argonne, IL 60439, United States

ARTICLE INFO

Article history:
Received 30 September 2019
Received in revised form 13 February 2020
Accepted 13 March 2020
Available online 14 March 2020

Keywords:
Single molecule conductance
Redox-active molecules
Molecular electronics
Intermolecular interactions
Scanning tunneling microscope break-junction (STM-BJ)

ABSTRACT

Intermolecular interactions play a key role in the charge transport properties of molecular electronic devices. In this work, we characterize charge transport in redox-active pyridinium-based molecular junctions mediated by host-guest interactions and intermolecular electrostatic effects. Charge transport through single pyridinium molecules generally shows that intramolecular conductance occurs over displacements consistent with the molecular contour length. However, pyridinium-based junctions exhibit charge transport over reduced molecular displacements upon increasing the solution concentration of the charged pyridinium complex, which is attributed to intermolecular electrostatic effects. Interestingly, formation of host-guest complexes via addition of a crown ether resulted in recovery of charge transport over molecular displacements corresponding to single pyridinium junctions at low concentrations, thereby suggesting that host-guest complexes efficiently screen electrostatic repulsions between cationic molecules. Bulk electrochemical characterization shows that pyridinium molecules exhibit stable redox-active properties over a wide array of conditions. Overall, this work opens new avenues for utilizing host-guest interactions that may be useful in informing the design of new redox-active flow batteries or programmable electronic devices.

1. Introduction

Understanding charge transport through redox-active molecules is of great interest for the design of redox flow batteries for grid-level energy storage [1,2]. Recent work has focused on a wide range of redox-active materials including oligomers [3], polymers [4,5], and colloidal particles [6], which are known to exhibit distinct physical and electrochemical properties based on chemical composition and size of molecular species. In tandem with bulk electrochemical characterization, the charge transport properties of redox-active species have recently been studied at the single molecule level [7]. To this end, integrating single molecule techniques with bulk electrochemical methods offers a particularly powerful approach for understanding fundamental charge transport mechanisms combined with device-scale performance.

In recent years, new methods in single molecule electronics have been used to understand intramolecular charge transport [8–11]. Molecular conductance and stochastic electron transfer reaction kinetics in redox-active molecules such as viologen [12], (2,2,6,6-tetramethylpiperidin-1-yl)oxyl (TEMPO) [13], phenothiazine [14], ferrocene [15], and thiophenylidene [16] derivatives were recently investigated, which is generally motivated by the development of promising applications in spintronics and molecular electronics. Moreover, prior work has also focused on the role of intermolecular interactions on charge transport. In particular, aromatic interactions [17,18], hydrogen bonding [19–21], Lewis acid-base interactions [22], host-guest interactions [12,23], and charge transfer complexation [24,25] have been explored and leveraged to design programmable molecular electronic devices. Despite recent progress, however, we still lack a complete understanding of the role of intermolecular interactions on charge transport in redox-active molecular junctions.

In this work, we characterize intermolecular interactions in redox-active pyridinium-based molecular junctions. Charge transport through single pyridinium molecules is observed over molecular displacements (0.74 ± 0.29 nm) consistent with the neutral control molecule (0.68 ± 0.17 nm). However, pyridinium-based junctions exhibit charge transport over reduced molecular displacements (0.33 ± 0.11 nm) upon increasing the solution concentration of the charged pyridinium molecule (10 mM), which is attributed to intermolecular electrostatic repulsions between pyridinium molecules in molecular junctions. Strikingly, formation of a host-guest complex via addition of a crown ether results in recovery of

* Corresponding author at: Department of Materials Science and Engineering, University of Illinois at Urbana-Champaign, Urbana, IL 61801, United States.
E-mail address: cms@illinois.edu. (C.M. Schroeder).
[1] Contributed equally to this work.

http://dx.doi.org/10.1016/j.jelechem.2020.114070

charge transport over a molecular displacement consistent with isolated pyridinium molecules at low solution concentration, which suggests that host-guest interactions can be used to shield electrostatic repulsions between cationic molecules in molecular junctions. Bulk electrochemical characterization including cyclic voltammetry and bulk electrolysis shows that pyridinium molecules exhibit stable redox-active properties across a range of experimental conditions. From a broad perspective, these results highlight the use of single molecule techniques to characterize the effect of intermolecular interactions on charge transport, which may aid in the design of new electrolytes for redox-active flow batteries with tunable electronic properties.

2. Experimental

2.1. General methods

2.1.1. Materials

Reagents were purchased from commercial suppliers and used as received unless otherwise stated. Dry dimethylformamide (DMF) is obtained from a solvent delivery system (SDS) equipped with activated neutral alumina columns under argon. Column-based chromatography was performed on a Biotage Isolera system using Siliasep flash cartridges (Silicycle).

2.1.2. NMR characterization

^{1}H and ^{13}C NMR spectra (500 MHz and 125 MHz) were recorded at room temperature (298 K). Chemical shifts are reported in δ (ppm) referenced on residual solvent peaks. Coupling constants (J) are expressed in Hertz (Hz). Splitting patterns are designated as: s (singlet), d (doublet), t (triplet), and m (multiplet).

2.1.3. Mass spectrometry

High-resolution electrospray ionization (ESI) and electron ionization (EI) mass spectra were recorded on a Waters Q-TOF Ultima ESI or Micromass 70-VSE EI spectrometer.

2.2. Chemical synthesis

1-(4-(Methylthio)phenyl)-[4,4′-bipyridin]-1-ium chloride (**V1**) is synthesized following a previously reported procedure [26]. 4-(4′-(methylthio)-[1,1′-biphenyl]-4-yl)pyridine (**V2**) was synthesized using the following protocol. Briefly, 4-bromo-4′-methylthiobiphenyl (500 mg, 1.80 mmol), 4-Pyridylboronic acid (220 mg, 1.80 mmol), $Pd(PPh_3)4$ (100 mg, 0.18 mmol), K_2CO_3 (990 mg, 7.22 mmol), degassed DMF (5.0 mL), and H_2O (0.5 mL) were added to a flame-dried flask. The reaction was heated to 80 °C and proceeded for 2 days. After cooling to room temperature, the mixture was poured into water (50 mL), extracted with dichloromethane (25 mL, 3×), and washed with water (50 mL) and brine (50 mL). The combined organic layers were dried over anhydrous sodium sulfate, filtered, and concentrated under reduced pressure. The product was purified by flash chromatography on silica gel with ethyl acetate to yield **V2** (120 mg, 24% yield) as a white solid. Following synthesis, purified materials were characterized using NMR (Figs. S1-S2): ^{1}H NMR (500 MHz, chloroform-*d*) δ 8.70 (d, J = 6.1 Hz, 2H), 7.78–7.69 (m, 4H), 7.63–7.55 (m, 4H), 7.38 (d, J = 8.4 Hz, 2H), 2.57 (s, 3H). ^{13}C NMR (125 MHz, chloroform-*d*) δ 150.35, 147.76, 141.29, 138.37, 136.89, 136.84, 127.46, 127.43, 127.39, 126.91, 121.42, 15.80. HRMS-ESI (m/z): C18H15NS [M + H]+; calculated: 278.1008, found: 278.1003.

2.3. Single molecule conductance

For single molecule conductance measurements, we used a custom scanning tunneling microscope-break junction (STM-BJ) instrument as previously described [10,16,27]. Briefly, the STM-BJ instrument consists of two working electrodes, such that a gold tip (0.25 mm Au wire, 99.998%, Alfa Aesar) is repeatedly driven into and out of contact with a gold substrate to form (and break) molecular junctions, thereby enabling measurement of conductance in molecular junctions. Experiments were performed under a constant applied bias of 250 mV at a tip pulling rate of 17 nm/s. Gold substrates were prepared by evaporating 120 nm of gold onto polished atomic force microscope (AFM) metal specimen discs (Ted Pella). Conductance measurements were carried out in a polar solvent (propylene carbonate). To minimize background ionic current, gold tips were coated with Apiezo wax to minimize the exposed contact area in solution [28]. In all cases, conductance measurements were performed over large molecular ensembles (5000–20,000 individual molecules) for robust statistical analysis. Molecular conductance traces were collected and analyzed without data selection.

2.4. Bulk electrochemical characterization

Bulk electrochemical experiments were conducted inside an argon-filled glove box, with oxygen and water levels strictly controlled at or below 0.1 ppm. Electrochemical measurements were performed using a potentiostat CHI760E with a 5 mM concentration of **V1** for cyclic voltammetry and 1 mM concentration of **V1** for bulk electrolysis in 0.1 M $TBAPF_6$ (supporting electrolyte) in propylene carbonate (PC). Voltammetry was carried out using a three-electrode configuration with a 1 mm radius Au disk macroelectrode or 12.5 μm radius Pt ultramicroelectrode (UME) as the working electrode, a non-aqueous Ag/Ag^+ reference electrode (0.1 M $AgNO_3$ in acetonitrile as $AgNO_3$ was insoluble in propylene carbonate), and a Pt wire as a counter electrode.

Potential-controlled bulk electrolysis of a stirred solution was carried out in a three-compartment W-cell divided by quartz frits (Adams & Chittenden). A carbon felt working electrode was placed in the middle compartment, and the two lateral compartments contained a Pt mesh counter electrode and the non-aqueous reference electrode. For bulk electrolysis of **V1**, the potential was held at −260 mV from $E_{1/2}$, and Pt UME voltammograms were obtained before and after the electrolysis to confirm complete reduction.

UV–vis spectroscopy was performed to characterize charged and uncharged species. To transfer the charged species from the drybox into the UV–vis spectrophotometer under ambient conditions, a UV–vis cuvette containing charged **V1**$^{\bullet}$ was specially treated to avoid reaction with oxygen that can result in **V1**$^{\bullet}$ discharge. In particular, under a dry argon atmosphere, a UV–vis cuvette containing 100 μM solution of charged **V1**$^{\bullet}$ species was tightly wrapped with multiple layers of Teflon tape, followed by two layers of electric tape. The cuvette was further placed into a glass jar, which acted as a temporary mobile argon chamber for transporting the sample through the ambient atmosphere. Reduced **V1**$^{\bullet}$ spectra show prominent peaks around 261, 400, and 560 nm, where the latter two are associated with the reduced form of viologens [3,29], whereas uncharged **V1**$^{+}$ displays peaks around 264 and 357 nm. The peaks at 260 and 400 nm are exhibited by both species, albeit with different intensities, whereas the peak at 560 nm is exclusive to the reduced species.

We also used a two-electrode STM-BJ system to perform cyclic voltammetry (CV) experiments on a solution of 1 mM **V1** and 0.1 M tetrabutylammonium hexafluorophosphate (electrolyte) in propylene carbonate at a scan rate of 100 mV/s from −1 to 1 V. These experiments were used to assess the redox state of **V1** during experiments and to ensure that **V1** remains in the cationic form during the single molecule conductance measurements.

3. Results and discussion

We began by measuring the conductance of 1-(4-(methylthio)phenyl)-[4,4′-bipyridin]-1-ium chloride (**V1**) and 4-(4′-(methylthio)-[1,1′-biphenyl]-4-yl)pyridine (**V2**) using the STM-BJ method under ambient conditions (Fig. 1a). In this way, **V1** and **V2** were synthesized to contain terminal methylthio [10] and pyridine groups [30] as chemical anchors to facilitate robust binding to the gold tip and substrate electrodes through lone pair interactions on the sulfur and nitrogen atoms in the methyl sulfide and pyridine groups, respectively. Single molecule conductance measurements were performed using two different concentrations (1 mM and 10 mM) of **V1** and **V2** in propylene carbonate. In the absence of molecules (pure solvent), the conductance is initially observed to decrease in steps as

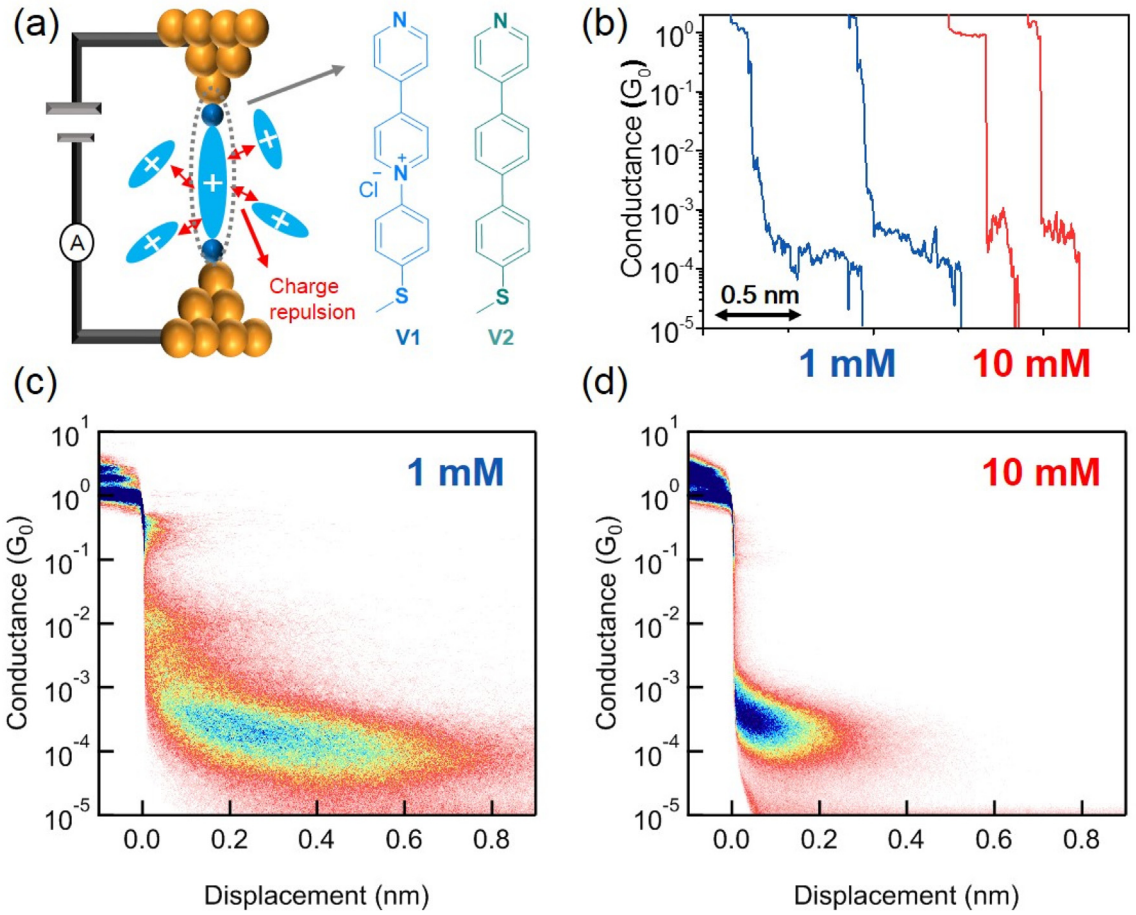

Fig. 1. Charge transport in pyridinium-based molecular junctions. (a) Schematic of gold-molecule-gold junction and molecular structures of **V1** and **V2**. (b) Characteristic single molecule conductance traces of **V1** (1 mM and 10 mM in propylene carbonate) at 0.25 V bias. (c-d) Two-dimensional (2D) conductance histograms for **V1** at 1 mM and 10 mM, determined over >5000 traces.

the gold tip is pulled away from the substrate, eventually dropping to a level below the detection limit of the instrument. Step-wise decrease in conductance in the absence of molecules corresponds multiple integers of the quantum conductance G_0 that reduce eventually to a single atom with single conductance channel [31], where $G_0 = 2e^2/h = 77.5$ μS, e is the electron charge, and h is Planck's constant.

Single molecule conductance experiments generally proceed in the following manner. In the presence of viologen molecules, a robust molecular junction is formed between the gold tip and substrate via the terminal anchor groups. As the tip is pulled away from the substrate, molecular conductance is measured under the application of an applied bias. Using this approach, we began by studying the charge transport properties of **V1**. A large fraction of single molecule conductance traces shows a plateau between 10^{-3} - 10^{-4} G_0, corresponding to charge transport through the pyridinium-based molecular junction (Fig. 1b). When the tip is pulled further away from the substrate, the molecular junction breaks down and the conductance drops below the detection limit of the instrument.

Single molecule conductance experiments are performed by repeating the process over large molecular ensembles to gather robust statistics. In this way, two-dimensional (2D) histograms of conductance versus tip displacement are generated over an ensemble of approximately 10^3–10^4 molecules without data selection. 2D conductance histograms for **V1** are shown in Fig. 1c-d for two different solution concentrations (1 mM and 10 mM). Interestingly, these results show that molecular conductance is measured over characteristic tip-substrate displacements as a function of solution concentration of **V1**. For these experiments, the tip-to-substrate separation is set to zero displacement when the metal contact breaks down, and the molecular conductance trajectory ends when the junction breaks. In this way, the relative tip-substrate displacement directly corresponds to the molecular junction length [32].

One-dimensional (1D) conductance histograms can be further constructed from single molecule conductance traces and analyzed with a Lorentzian function to determine the average molecular conductance. Our results show that the average molecular conductance of **V1** is 2.2×10^{-4} G_0 at 10 mM, which is approximately twice the average conductance of **V1** at 1 mM (Fig. 2a). We conjecture that this relatively small increase in average conductance arises due to intermolecular aromatic interactions between the phenyl ring spacer in the molecule, which has also been observed in prior work on conjugated aromatic systems [33]. To further analyze the conductance behavior, we constructed tip-substrate displacement histograms and determined the arithmetic mean displacements (or lengths) of molecular junctions. In particular, mean lengths of molecular junctions were calculated by determining the relative distance between tip-substrate displacement at a molecular conductance of 0.5 G_0 (corresponding to a stretched molecular junction) and the conductance corresponding to 10% of the average junction conductance calculated from 1D histograms (corresponding to the junction break point) [32]. Using this approach, displacement histograms were determined for **V1** in 1 mM and 10 mM solutions (Fig. 2b). Our results show that at a concentration of 1 mM, molecular junctions based on **V1** can be stretched to displacements of 0.74 ± 0.29 nm, which is consistent with the non-redox active counterpart molecule **V2** (Fig. S3). Moreover, the average length of molecular junctions based on **V1** remains nearly constant, even at significantly lower concentrations of **V1** (0.01 mM) (Fig. S4). Interestingly, we observed that the molecular displacements of **V2** are essentially unchanged at a concentration of 10 mM (Fig. S3), which generally precludes concentration-dependent surface

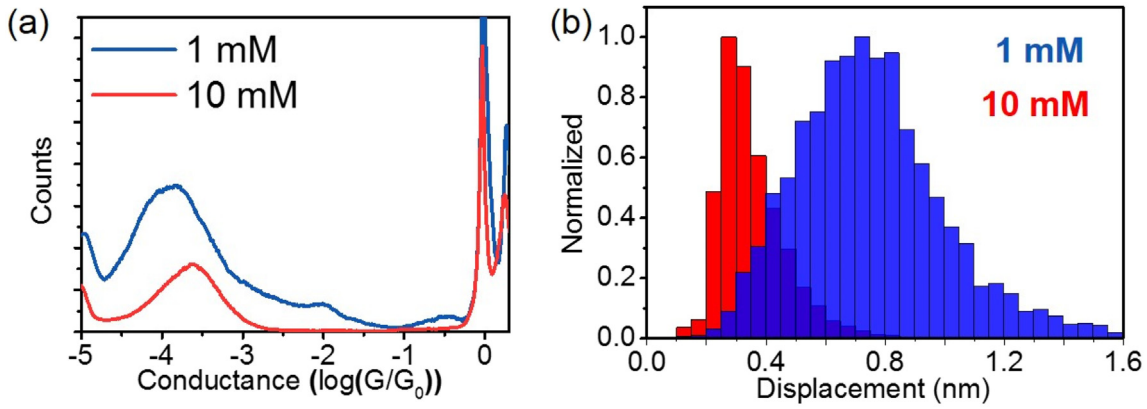

Fig. 2. Molecular conductance and junction displacements for **V1**. (a) 1D conductance histograms for **V1** with 1 mM and 10 mM concentrations at 0.25 V bias (>5000 traces for each). (b) Molecular junction displacement distributions for **V1** at 1 mM and 10 mM.

coverage effects in altering molecular displacements. However, molecular junction lengths for **V1** significantly decreased to 0.33 ± 0.11 nm at a concentration of 10 mM. Importantly, the decrease in molecular junction length indicates that intermolecular interactions may be affecting conductance measurements due to electrostatic charge repulsion. For this analysis, we determined that the criterion for defining junction end point rupture does not significantly affect the final displacement results within a range of 4% to 20% of the average junction conductance (Fig. S5). Molecular conductance at end points < 4% of the average junction conductance was disregarded due to proximity to the detection limit of the STM-BJ instrument.

In general, the intramolecular conductance pathway is not expected to depend on the solution concentration of **V1** over the relatively small range of 1–10 mM. In addition, prior work has shown that surface coverage is saturated for molecules terminated with methylthio and pyridine at concentrations above 1 mM [34]. From this view, the change in molecular junction length can be explained by the variation in junction stability due to intermolecular interactions between **V1** molecules in solution. We posit that pyridinium-based molecules can be stretched to near full extension in low concentration solutions of **V1**. However, upon increasing the solution concentration of **V1**, intermolecular interactions due to electrostatic repulsion between pyridinium cations hinder the stretching process in pyridinium molecular junctions. In this way, cationic repulsions in solution destabilize the molecular junction, ultimately resulting in junction rupture before stretching to full extension.

To test this hypothesis, we utilized host-guest chemistry to minimize electrostatic repulsions between pyridinium cations in solution. The supramolecular chemistry enabled by crown ether-based host-guest systems has attracted substantial attention because of potential applications in developing molecular devices and functional supramolecular materials [35]. Host-guest complexes form when a cationic guest molecule binds to a neutral host molecule such as crown ether through non-covalent interactions [23,36]. Previous studies have shown that the stable 1:1 host-guest inclusion complexes can be formed and stabilized between benzene-substituted crown ethers and electron-deficient pyridinium cations through both π-π and cation-π interactions [37]. To assess the formation of host-guest complexes, UV–vis spectra of **V1** with or without **C1** and **C2** were determined. Upon the addition of **C1** and **C2**, there is a small shift in the peak of the absorption band from 264 nm to 261 nm and a decrease in absorption (Fig. S6). The decrease in the wavelength of the absorption peak is consistent with prior work for other pyridinium-based host-guest systems and has been used as evidence supporting the formation of host-guest complexes [12]. In this way, we used a similar host-guest molecular system to shield the positively charged pyridinium cations in **V1** molecular junctions. Remarkably, our results show that formation of host-guest complexes minimize intermolecular charge repulsions, thereby recovering fully stretched molecular junctions in 10 mM concentration solutions of **V1** (Fig. 3b).

Host-guest molecular conductance experiments were performed by adding 10 mM of dibenzo-24-crown-8 (**C1**) into 10 mM solutions of **V1**, followed by direct measurement of molecular conductance using the STM-BJ instrument. Our results show a that host-guest complexes of **C1** + **V1** exhibit high levels of molecular conductance over junction lengths of 0.67 ± 0.19 nm, which corresponds to junction lengths of **V1** in low concentrations. Interestingly, the average molecular conductance for **C1** + **V1** host-guest complexes was equivalent to the conductance of **V1** at 10 mM solution concentration (Figs. 3c and S7). Moreover, we found that the size of the macrocycle cavity did not generally influence the screening of electrostatic repulsions between cations in solution. In particular, host-guest complexes between **V1** and larger size crown ethers such as dibenzo-30-crown-10 (**C2**), we found that molecular junctions achieved the same junction length (0.70 ± 0.19 nm) compared to the smaller size crown ether **C1** (Fig. 3d). In general, our results show that host-guest complex formation is capable of screening intermolecular cationic repulsions between nearby pyridinium molecules, thereby yielding similar junction lengths for host-guest complexes in high concentration (10 mM) compared to isolated **V1** molecules in low concentration (1 mM) solutions. In addition, we observe no evidence of stable junction formation in solutions containing only crown ether (Fig. S8). Moreover, we did not observe differences in molecular displacements upon addition of 10 mM **C1** or **C2** into 10 mM neutral **V2** solutions (Fig. S9). Overall, these findings are consistent with our hypothesis intermolecular repulsions induce junction instabilities during molecular stretching.

In order to assess if the obtained STM-BJ experiments were affected by the stability of **V1**'s redox states, we performed a series of bulk electrochemical experiments. As previously noted, pyridinium-based molecules such as **V1** are redox-active. Therefore, we performed a series of cyclic voltammetry (CV) experiments to ensure that **V1** is not undergoing electrochemical activity within the range of the applied bias (0–0.25 V). Our results show that **V1** remains in the cationic form under these experimental conditions (Fig. S10). Fig. 4a shows a cyclic voltammogram for a 5 mM solution of **V1** in 0.1 M $TBAPF_6$ in propylene carbonate at a scan rate of 5 mV/s on a Au disk macroelectrode (2 mm radius) under an argon atmosphere. The electrochemical response of **V1** at low scan rates demonstrates a reversible reduction of $\mathbf{V1}^+$ to $\mathbf{V1}^{\bullet}$, centered at −1.14 V versus Ag/Ag^+, with peak current ratios near unity. Scan-rate dependent CV experiments in Fig. S11 showed linearity of the peak current vs. square root of scan rate, indicating diffusional control of V1's reactivity at the electrode. Bulk electrolysis and UV–vis spectroscopy characterization of both the initial and reduced species, are shown in Figs. 4b and S12. Here, a 1 mM solution of **V1** was electrolyzed at an overpotential of −1.4 V versus Ag/Ag^+ to the state of charge of 1.0, where the charging current dropped to < 1% of the initial current. A change in color from clear pale yellow to clear burgundy was observed as the solution was charging (Fig. 4b). In order to assess the extent of **V1** charging in solution, cyclic

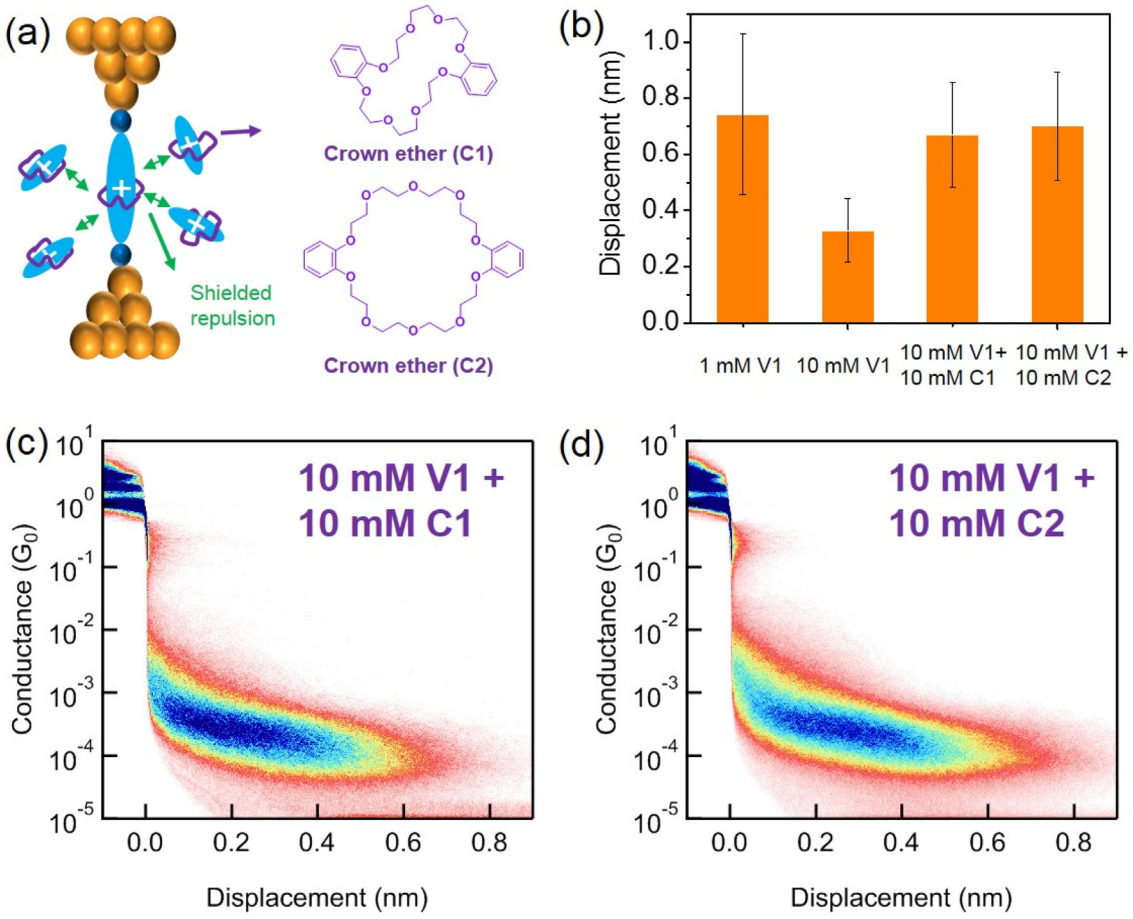

Fig. 3. Molecular conductance and displacement of pyridinium-crown ether complex. (a) Schematic of shielded charge repulsion in molecular junction through complex formation between pyridinium (**V1**) and crown ether (**C1**, **C2**). (b) Average molecular displacement at different conditions of **V1** and crown ether. (c-d) Two-dimensional (2D) conductance histograms for 10 mM **V1** with 10 mM **C1** and 10 mM **C2** at 0.25 V bias.

voltammograms using platinum ultramicroelectrode (UME) were obtained prior to charging and immediately following the charging process, as shown in Fig. 4b. UME voltammetric waves for both uncharged and charged species exhibit a sigmoidal shape and generally achieve a steady-state current, as expected for a facile charge transfer at the microelectrode. The UME voltammograms reveal that the charged species produces nearly equal amounts of steady-state current compared to the uncharged species, further demonstrating that **V1** does not undergo decomposition while charging, and thus, unlikely during STM-BJ experiments.

4. Conclusion

In summary, we use single molecule techniques to characterize intermolecular interactions in redox-active pyridinium-based molecular junctions. We observe that the molecular displacement through different

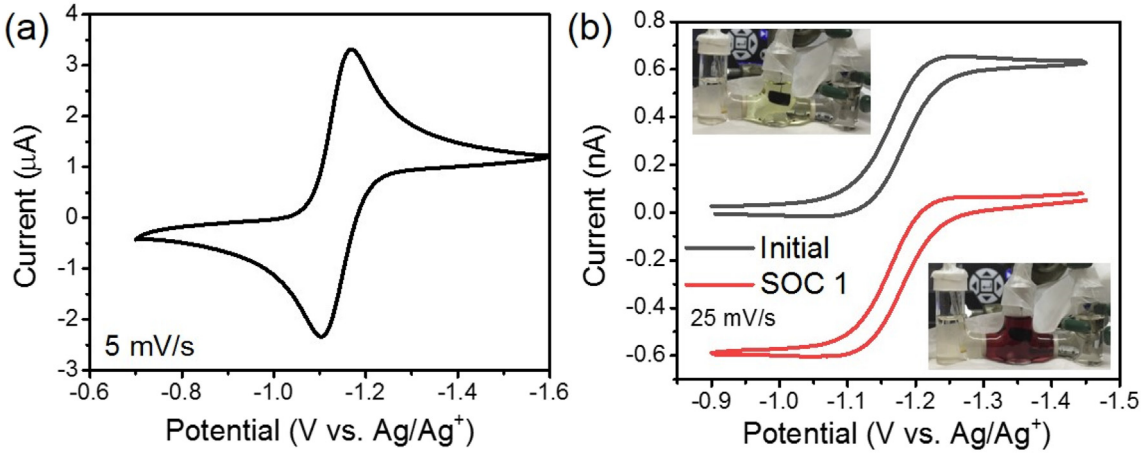

Fig. 4. Bulk electrochemical characterization of pyridinium-based molecule **V1**. (a) Cyclic voltammogram for a 5 mM solution of **V1** in 0.1 M $TBAPF_6$ in propylene carbonate at a scan rate of 5 mV/s on a Au disk macroelectrode (2 mm radius) under an argon atmosphere. (b) Bulk electrolysis characterization of the initial **V1** and reduced species **V1**$^{\bullet}$.

concentrations of pyridinium molecules exhibits strikingly large differences compared to neutral control molecules. Addition of crown ethers induces formation of host-guest complexes and screens charge repulsion, thereby resulting in conductance measured over molecular displacements consistent with the full-length molecules. Taken together, these results show that intermolecular interactions play an essential role in charge transport of molecular junctions. Bulk electrochemical experiments including cyclic voltammetry and electrolysis clearly demonstrate that the pyridinium molecules exhibit stable and reversible redox-active properties.

Recently, several studies have shown that redox-active molecules exhibit characteristic molecular conductance signatures as a function of the redox state. From this view, application of external gate voltage can be used to tune the redox state of a molecular junction, thereby serving as an efficient molecular switch for modulating charge transport [14,16]. Pyridinium molecules with stable and reversible redox-active properties are capable to change redox states under various external gate voltages. Our results suggest that pyridinium-based molecules could be used in the design and development tunable redox-active materials or switchable molecular electronics.

CRediT authorship contribution statement

Songsong Li: Conceptualization, Investigation, Writing - original draft. **Jialing Li:** Investigation, Validation, Software, Writing - original draft. **Hao Yu:** Investigation, Resources. **Sanja Pudar:** Investigation, Writing - original draft. **Bo Li:** Investigation, Resources. **Joaquín Rodríguez-López:** Supervision. **Jeffrey S. Moore:** Supervision. **Charles M. Schroeder:** Supervision, Writing - original draft, Writing - review & editing.

Declaration of competing interest

The authors declare that they have no known competing financial interests or personal relationships that could have appeared to influence the work reported in this paper.

Acknowledgements

The research was financially supported by the Joint Center for Energy Storage Research (JCESR), an Energy Innovation Hub funded by the U.S. Department of Energy, Office of Science, Basic Energy Sciences.

Appendix A. Supplementary data

Supplementary data to this article can be found online at https://doi.org/10.1016/j.jelechem.2020.114070.

References

[1] W. Wang, Q. Luo, B. Li, X. Wei, L. Li, Z. Yang, Recent progress in redox flow battery research and development, Adv. Funct. Mater. 23 (2013) 970–986.
[2] M. Burgess, J.S. Moore, J. Rodríguez-López, Redox active polymers as soluble nanomaterials for energy storage, Acc. Chem. Res. 49 (2016) 2649–2657.
[3] M. Burgess, E. Chénard, K. Hernández-Burgos, G. Nagarjuna, R.S. Assary, J. Hui, J.S. Moore, J. Rodríguez-López, Impact of backbone tether length and structure on the electrochemical performance of viologen redox active polymers, Chem. Mater. 28 (2016) 7362–7374.
[4] G. Nagarjuna, J. Hui, K.J. Cheng, T. Lichtenstein, M. Shen, J.S. Moore, J. Rodríguez-López, Impact of redox-active polymer molecular weight on the electrochemical properties and transport across porous separators in nonaqueous solvents, J. Am. Chem. Soc. 136 (2014) 16309–16316.
[5] T. Janoschka, N. Martin, U. Martin, C. Friebe, S. Morgenstern, H. Hiller, M.D. Hager, U.S. Schubert, An aqueous, polymer-based redox-flow battery using non-corrosive, safe, and low-cost materials, Nature 527 (2015) 78.
[6] E.C. Montoto, G. Nagarjuna, J. Hui, M. Burgess, N.M. Sekerak, K. Hernández-Burgos, T.-S. Wei, M. Kneer, J. Grolman, K.J. Cheng, Redox active colloids as discrete energy storage carriers, J. Am. Chem. Soc. 138 (2016) 13230–13237.
[7] R.J. Nichols, S.J. Higgins, Single molecule nanoelectrochemistry in electrical junctions, Acc. Chem. Res. 49 (2016) 2640–2648.
[8] B. Xu, N.J. Tao, Measurement of single-molecule resistance by repeated formation of molecular junctions, Science 301 (2003) 1221–1223.
[9] L. Venkataraman, J.E. Klare, C. Nuckolls, M.S. Hybertsen, M.L. Steigerwald, Dependence of single-molecule junction conductance on molecular conformation, Nature 442 (2006) 904.
[10] B. Li, H. Yu, E.C. Montoto, Y. Liu, S. Li, K. Schwieter, J. Rodríguez-López, J.S. Moore, C.M. Schroeder, Intrachain charge transport through conjugated donor–acceptor oligomers, ACS Appl. Electron. Mater. 1 (2018) 7–12.
[11] N. Xin, J. Guan, C. Zhou, X. Chen, C. Gu, Y. Li, M.A. Ratner, A. Nitzan, J.F. Stoddart, X. Guo, Concepts in the design and engineering of single-molecule electronic devices, Nature Rev. Phys. 1 (2019) 211–230.
[12] W. Zhang, S. Gan, A. Vezzoli, R.J. Davidson, D.C. Milan, K.V. Luzyanin, S.J. Higgins, R.J. Nichols, A. Beeby, P.J. Low, Single-molecule conductance of viologen–cucurbit [8] uril host–guest complexes, ACS Nano 10 (2016) 5212–5220.
[13] R. Hayakawa, M.A. Karimi, J. Wolf, T. Huhn, M.S. Zöllner, C. Herrmann, E. Scheer, Large magnetoresistance in single-radical molecular junctions, Nano Lett. 16 (2016) 4960–4967.
[14] J. Liu, X. Zhao, Q. Al-Galiby, X. Huang, J. Zheng, R. Li, C. Huang, Y. Yang, J. Shi, D.Z. Manrique, Radical-enhanced charge transport in single-molecule phenothiazine electrical junctions, Angew. Chem. Int. Ed. 56 (2017) 13061–13065.
[15] Y. Li, H. Wang, Z. Wang, Y. Qiao, J. Ulstrup, H.-Y. Chen, G. Zhou, N. Tao, Transition from stochastic events to deterministic ensemble average in electron transfer reactions revealed by single-molecule conductance measurement, Proc. Natl. Acad. Sci. 116 (2019) 3407–3412.
[16] X. Yin, Y. Zang, L. Zhu, J.Z. Low, Z.-F. Liu, J. Cui, J.B. Neaton, L. Venkataraman, L.M. Campos, A reversible single-molecule switch based on activated antiaromaticity, Sci. Adv. 3 (2017) eaao2615.
[17] S. Fujii, T. Tada, Y. Komoto, T. Osuga, T. Murase, M. Fujita, M. Kiguchi, Rectifying electron-transport properties through stacks of aromatic molecules inserted into a self-assembled cage, J. Am. Chem. Soc. 137 (2015) 5939–5947.
[18] R. Frisenda, V.A. Janssen, F.C. Grozema, H.S. van der Zant, N. Renaud, Mechanically controlled quantum interference in individual π-stacked dimers, Nat. Chem. 8 (2016) 1099.
[19] T. Nishino, N. Hayashi, P.T. Bui, Direct measurement of electron transfer through a hydrogen bond between single molecules, J. Am. Chem. Soc. 135 (2013) 4592–4595.
[20] L. Wang, Z.L. Gong, S.Y. Li, W. Hong, Y.W. Zhong, D. Wang, L.J. Wan, Molecular conductance through a quadruple-hydrogen-bond-bridged supramolecular junction, Angew. Chem. Int. Ed. 55 (2016) 12393–12397.
[21] C. Zhou, X. Li, Z. Gong, C. Jia, Y. Lin, C. Gu, G. He, Y. Zhong, J. Yang, X. Guo, Direct observation of single-molecule hydrogen-bond dynamics with single-bond resolution, Nat. Commun. 9 (2018) 807.
[22] X. Liu, X. Li, S. Sangtarash, H. Sadeghi, S. Decurtins, R. Häner, W. Hong, C.J. Lambert, S.-X. Liu, Probing Lewis acid–base interactions in single-molecule junctions, Nanoscale 10 (2018) 18131–18134.
[23] H. Wen, W. Li, J. Chen, G. He, L. Li, M.A. Olson, A.C.-H. Sue, J.F. Stoddart, X. Guo, Complex formation dynamics in a single-molecule electronic device, Sci. Adv. 2 (2016), e1601113.
[24] A. Vezzoli, I. Grace, C. Brooke, K. Wang, C.J. Lambert, B. Xu, R.J. Nichols, S.J. Higgins, Gating of single molecule junction conductance by charge transfer complex formation, Nanoscale 7 (2015) 18949–18955.
[25] K. Wang, A. Vezzoli, I.M. Grace, M. McLaughlin, R.J. Nichols, B. Xu, C.J. Lambert, S.J. Higgins, Charge transfer complexation boosts molecular conductance through Fermi level pinning, Chem. Sci. 10 (2019) 2396–2403.
[26] M.C. Rezende, I. Ponce, R. Oñate, I. Almodovar, C. Aliaga, Change of mechanism with a change of substituents for a Zincke reaction, Tetrahedron Lett. 55 (2014) 3097–3099.
[27] S. Li, H. Yu, K. Schwieter, K. Chen, B. Li, Y. Liu, J.S. Moore, C.M. Schroeder, Charge transport and quantum interference effects in oxazole-terminated conjugated oligomers, J. Am. Chem. Soc. 141 (2019) 16079–16084.
[28] L.A. Nagahara, T. Thundat, S.M. Lindsay, Preparation and characterization of STM tips for electrochemical studies, Rev. Sci. Instrum. 60 (1989) 3128–3130.
[29] B. Gadgil, E. Dmitrieva, P. Damlin, T. Ääritalo, C. Kvarnström, Redox reactions in a linear polyviologen derivative studied by in situ ESR/UV-vis-NIR spectroelectrochemistry, J. Solid State Electrochem. 19 (2015) 77–83.
[30] M. Kamenetska, S.Y. Quek, A. Whalley, M. Steigerwald, H. Choi, S.G. Louie, C. Nuckolls, M. Hybertsen, J. Neaton, L. Venkataraman, Conductance and geometry of pyridine-linked single-molecule junctions, J. Am. Chem. Soc. 132 (2010) 6817–6821.
[31] L. Venkataraman, J.E. Klare, I.W. Tam, C. Nuckolls, M.S. Hybertsen, M.L. Steigerwald, Single-molecule circuits with well-defined molecular conductance, Nano Lett. 6 (2006) 458–462.
[32] P. Moreno-García, M. Gulcur, D.Z. Manrique, T. Pope, W. Hong, V. Kaliginedi, C. Huang, A.S. Batsanov, M.R. Bryce, C. Lambert, Single-molecule conductance of functionalized oligoynes: length dependence and junction evolution, J. Am. Chem. Soc. 135 (2013) 12228–12240.
[33] A. Magyarkuti, O. Adak, A. Halbritter, L. Venkataraman, Electronic and mechanical characteristics of stacked dimer molecular junctions, Nanoscale 10 (2018) 3362–3368.
[34] C. Zhan, G. Wang, X.-G. Zhang, Z.-H. Li, J.-Y. Wei, Y. Si, Y. Yang, W. Hong, Z.-Q. Tian, Single-molecule measurement of adsorption free energy at the solid–liquid interface, Angew. Chem. 131 (2019) 14676–14680.
[35] M. Zhang, X. Yan, F. Huang, Z. Niu, H.W. Gibson, Stimuli-responsive host–guest systems based on the recognition of cryptands by organic guests, Acc. Chem. Res. 47 (2014) 1995–2005.
[36] H.R. Wessels, C. Slebodnick, H.W. Gibson, Viologen-based rotaxanes from dibenzo-30-crown-10, J. Am. Chem. Soc. 140 (2018) 7358–7370.
[37] M. Lämsä, J. Huuskonen, K. Rissanen, J. Pursiainen, X-ray and NMR studies on host–guest inclusion complex formation between crown ethers and pyridinium compounds, Chem. Eur. J. 4 (1998) 84–92.